Paired MEG Data Set Source Localization Using Recursively Applied and Projected (RAP) MUSIC

John J. Ermer, *Member, IEEE*, John C. Mosher, *Member, IEEE*, Mingxiong Huang, and Richard M. Leahy*, *Member, IEEE*

***Abstract*—An important class of experiments in functional brain mapping involves collecting pairs of data corresponding to separate "Task" and "Control" conditions. The data are then analyzed to determine what activity occurs during the Task experiment but not in the Control. Here we describe a new method for processing paired magnetoencephalographic (MEG) data sets using our recursively applied and projected multiple signal classification (RAP-MUSIC) algorithm. In this method the signal subspace of the Task data is projected against the orthogonal complement of the Control data signal subspace to obtain a subspace which describes spatial activity unique to the Task. A RAP-MUSIC localization search is then performed on this projected data to localize the sources which are active in the Task but not in the Control data. In addition to dipolar sources, effective blocking of more complex sources, e.g., multiple synchronously activated dipoles or synchronously activated distributed source activity, is possible since these topographies are well-described by the Control data signal subspace. Unlike previously published methods, the proposed method is shown to be effective in situations where the time series associated with Control and Task activity possess significant cross correlation. The method also allows for straightforward determination of the estimated time series of the localized target sources. A multiepoch MEG simulation and a phantom experiment are presented to demonstrate the ability of this method to successfully identify sources and their time series in the Task data.**

***Index Terms*—Array signal processing, magnetoencephalography, signal subspace methods, source localization.**

I. Introduction

TO ISOLATE the components of the complex processes involved in sensorimotor and cognitive brain activation, brain imaging studies are often performed to examine the difference in response between a baseline or "Control" condition and a specific "Task" condition. In positron emission tomography (PET) and functional magnetic resonance imaging (fMRI) activation studies, differences between the two conditions are determined using methods ranging from simple image subtraction to sophisticated statistical analysis of differences between sets of Control and Task images [1]. Equivalently, magnetoencephalography (MEG) data could be analyzed by separately estimating all sources in the Control and Task data and then performing a statistical analysis of the differences between the two. However, when using nonlinear localization or imaging methods, the accuracy with which sources can be estimated decreases with increasing complexity of the sources [2]. This has motivated a number of researchers to investigate methods for estimating only those sources which are present in the Task but not in the Control data.

Variations in latency from epoch to epoch will result in differences between two data sets even when the sources in the two data sets are nominally the same. Consequently, as shown in [3], simple waveform subtraction between Task and Control data-sets fails if there is any latency variation in the common source activity between the two sets of data. Sekihara *et al.* [3] describe an alternative method based on a covariance difference algorithm. In this method, a MUSIC localization search ([4], [5]) is performed using the subspace of the difference matrix formed by the subtraction of the Control covariance matrix from the Task covariance matrix. One of the underlying assumptions in this method is that the cross correlation between the Control and Task source time series is zero. This method was shown to be effective at blocking out Control sources (and localizing target sources) in cases where cross correlation between Task and Control source time-series was minimal (i.e., the cross correlation was less than 0.3). However, in situations where significant cross correlation exists between the time series of Control and Target sources, this method was ineffective. Another limitation of this method was that it did not allow for straightforward estimation of the time-series associated with localized target activity.

Soong and Koles [6] present a method based on principal components for localizing abnormal components contained in the electroencephalographic (EEG) data. The method is based on the assumption that the covariance matrix can be expressed as the sum of a standard control EEG and a second EEG containing abnormal components. Spike and sharp wave potentials (representing the abnormal activity of interest) are identified visually based on the morphology of the waveforms corresponding to each of the common spatial patterns. An EEG is then reconstructed from these components, this is followed by localization on the reconstructed EEG data-set. One feature of this

Manuscript received November 9, 1998; revised May 15, 2000. This work was supported in part by the National Institute of Mental Health under Grant R01-MH53213, by Los Alamos National Laboratory, operated by the University of California for the United States Department of Energy, under Contract W-7405-ENG-36, and by the Raytheon Doctoral Fellowship Program. *Asterisk indicates corresponding author.*

J. J. Ermer is with the Signal & Image Processing Institute, University of Southern California, Los Angeles, CA 90089-2564 USA. He is also with Raytheon Systems Company, El Segundo, CA 90245 USA (e-mail: ermer@SIPI.USC.Edu).

J. C. Mosher is with Los Alamos National Laboratory, Los Alamos, NM 87545 USA (e-mail: mosher@LANL.Gov).

M. Huang is with the University of New Mexico, Albuquerque, NM 87131 USA (e-mail: mhuang@UNM.Edu).

*R. M. Leahy is with the Signal & Image Processing Institute, University of Southern California, Los Angeles, CA 90089-2564 USA (e-mail: leahy@SIPI.USC.Edu).

Publisher Item Identifier S 0018-9294(00)08014-9.

method is that it allows for reconstruction of the time series associated with the "abnormal" target activity. As was the case in [3], this method operates under the implicit assumption that Control (normal) and Task (abnormal) activity are uncorrelated.

Here, we present an alternative method for determining the sources spatially unique to the Task data. The method represents an extension to the RAP-MUSIC algorithm in which the signal subspace of the Control data is estimated and its orthogonal complement computed. The signal subspace of the Task data is then projected into the orthogonal complement of the Control data signal subspace to obtain a subspace which describes activity unique to the Task data. A standard RAP-MUSIC search is then performed to estimate the Task source parameters. In contrast to the methods in [3] and [6], this method does not require that the sources unique to the Task data set be uncorrelated with those in the Control. Furthermore, the method allows accurate extraction of the associated time series. One of the other advantages of this and other subspace-based methods is that complex source distributions in the Control data can be represented directly from their measurement signal subspace without resorting to specific assumptions or models.

The layout of paper is as follows. Section II provides the basic definitions and an overview of the RAP-MUSIC algorithm. A description of the proposed method is presented in Section III. Results from a multiepoch Monte Carlo simulation and phantom study are presented in Sections IV and V, respectively. Final conclusions are drawn in Section VI.

The notation used throughout this paper is as follows. In general, an italicized plain font is used to denote scalar quantities, and boldface is used to indicate column vectors and matrices. The superscript "T" is used to denote the transpose operator. For any matrix or vector, the subscripts "C," "T," and "D" are used to denote Control, Task, and Distinct Task (i.e., sources in "T" but not in "C"), respectively.

II. Background

A. The Forward Model

The objective of MEG inverse methods is to estimate neural current source characteristics given an observed set of noise-corrupted magnetic field measurements. For the biological signals of interest in MEG, the time-derivatives of the associated electric and magnetic fields are sufficiently small that the fields may be considered quasistatic (e.g., [7] and [8]). Under the quasistatic approximation, the magnetic field resulting from an arbitrary static current distribution (e.g., discrete dipoles, multiple synchronously activated dipoles, synchronously activated current fields, or combinations thereof) can be determined using the Biot–Sarvart law. The inverse problem can be solved by inverting the Biot–Savart law; unfortunately, the solution is not unique. That is, an infinite number of source configurations inside the brain can account for a given set of magnetic field measurements. The problem is often further complicated by the limited number of measurements available. As a result, physical models for the underlying current distribution are employed [8]. Here we will restrict ourselves to distinct Task sources that can be well modeled as collections of equivalent current dipoles.

The *forward model* relates a current dipole of moment $\boldsymbol{q}$ at location $\boldsymbol{r_q}$ to the magnetic field $\boldsymbol{b}(\boldsymbol{r})$ at location $\boldsymbol{r}$. This "primary" current generates volume (or "return") currents that must also be included in the forward model. We will limit our discussion here to the case of spherically symmetric head models for which closed form solutions of the forward problem are well known. See [9] for a review of other forward models in EEG and MEG and explicit formulations in the linear algebraic framework used here.

The general expression for the magnetic field outside a spherically symmetric volume is given by Sarvas [10]. For the special case where the MEG sensor is radially oriented, the contribution due to passive volume currents in the spherical model will vanish, and the forward model simplifies to the following well-known result

$$b(\boldsymbol{r}) = \frac{\mu_0}{4\pi} \cdot \frac{\boldsymbol{r} \times \boldsymbol{r_q}}{d^3 r} \cdot \boldsymbol{q} \tag{1}$$

where d is the distance between the observation and source locations, $d = |\boldsymbol{r} - \boldsymbol{r_q}|$. Regardless of the specifics of the forward model, by electromagnetic superposition the forward model is linear in the moment, and we may write the relationship between the dipole moment and the sensor measurement as the inner product of a "lead field" vector and the moment, $b(\boldsymbol{r}) = \boldsymbol{g}(\boldsymbol{r}, \boldsymbol{r}_q) \cdot \boldsymbol{q}$.

We assume an MEG array of m sensors sampling the magnetic field of the dipole. By concatenating the measurements into a vector, we can represent the "forward field" of the dipole as

$$\begin{bmatrix} b(\boldsymbol{r}_1) \\ \cdots \\ b(\boldsymbol{r}_m) \end{bmatrix} = \begin{bmatrix} \boldsymbol{g}(\boldsymbol{r}_1, \boldsymbol{r_q})^T \\ \cdots \\ \boldsymbol{g}(\boldsymbol{r}_m, \boldsymbol{r_q})^T \end{bmatrix} \boldsymbol{q} = \boldsymbol{G}(\boldsymbol{r_q})\boldsymbol{q} \tag{2}$$

where the "gain matrix" $\boldsymbol{G}(\boldsymbol{r_q})$ is also a function of the set of discrete sensor locations $\{\boldsymbol{r}_i\}$.

B. Independent Topographies

To maintain consistency with our terminology in [11], we define a *p-dipole independent topography* as a set of p dipoles having the same quasistatic time course. For any arbitrary set of p dipoles, the forward model can be found by summing (2) over all dipole locations $\{\boldsymbol{r_{qj}}\}$ and moments $\{\boldsymbol{q}_j\}$, $j = 1, \ldots, p$. For an independent topography sampled over m sensors and n time instances, we can express the resulting $m \times n$ spatiotemporal data matrix as

$$\begin{bmatrix} b(\boldsymbol{r}_1, \boldsymbol{t}_1) & \cdots & b(\boldsymbol{r}_1, \boldsymbol{t}_n) \\ \cdots & \cdots & \cdots \\ b(\boldsymbol{r}_m, \boldsymbol{t}_1) & \cdots & b(\boldsymbol{r}_m, \boldsymbol{t}_n) \end{bmatrix} = [\boldsymbol{G}(\boldsymbol{r_{q1}}) \quad \cdots \quad \boldsymbol{G}(\boldsymbol{r_{qp}})] \begin{bmatrix} \boldsymbol{q}_1(t_1) & \cdots & \boldsymbol{q}_1(t_n) \\ \cdots & \cdots & \cdots \\ \boldsymbol{q}_p(t_1) & \cdots & \boldsymbol{q}_p(t_n) \end{bmatrix} \tag{3}$$

where $\boldsymbol{q}_j(t_k)$ represents the jth dipole sampled at the kth time instance.

By definition of a p-dipole topography, all of these dipoles have the same time course and therefore the matrix of dipole moments in (3) is rank one. A singular value decomposition (SVD) yields a single nonzero singular value σ and the corresponding set of singular vectors $\boldsymbol{u}$ and $\boldsymbol{v}$, such that the dipole moments matrix is represented as

$$\boldsymbol{u}\sigma\boldsymbol{v}^T = \begin{bmatrix} \boldsymbol{q}_1(t_1) & \cdots & \boldsymbol{q}_1(t_n) \\ \cdots & \cdots & \cdots \\ \boldsymbol{q}_p(t_1) & \cdots & \boldsymbol{q}_p(t_n) \end{bmatrix}. \tag{4}$$

Defining the scalar time series of this independent topography to be $\boldsymbol{s} = \sigma\boldsymbol{v}$, we can rewrite (3) as

$$[\boldsymbol{G}(\boldsymbol{r}_{\boldsymbol{q}1}) \quad \cdots \quad \boldsymbol{G}(\boldsymbol{r}_{\boldsymbol{q}p})]\,\boldsymbol{u}\,[s(t_1) \quad \cdots \quad s(t_n)] = \boldsymbol{a}(\rho, \boldsymbol{u})\boldsymbol{s}^T. \tag{5}$$

The p-dipolar topography vector $\boldsymbol{a}(\rho, \boldsymbol{u}) \equiv \boldsymbol{G}(\rho)\boldsymbol{u}$ is a function of the set ρ of p dipole locations, $\rho = \{\boldsymbol{r}_{\boldsymbol{q}j}\}$ and the unit norm vector $\boldsymbol{u}$ from (4). The vector $\boldsymbol{u}$ can be viewed as a generalization of an "orientation" vector by alternatively concatenating all of the dipolar moments and scaling by the resulting vectors norm

$$\boldsymbol{u} \equiv [\boldsymbol{q}_1^T \quad \cdots \quad \boldsymbol{q}_p^T]\,/\,\|[\boldsymbol{q}_1^T \quad \cdots \quad \boldsymbol{q}_p^T]\|. \tag{6}$$

The full forward model considered here comprises r independent topographies in the presence of noise producing the measurement matrix

$$\begin{aligned} \boldsymbol{F} &= \boldsymbol{A}(\rho, \boldsymbol{u})\boldsymbol{S}^T + \boldsymbol{N} \\ &= [\boldsymbol{a}(\rho_1, \boldsymbol{u}_1) \quad \cdots \quad \boldsymbol{a}(\rho_r, \boldsymbol{u}_r)] \begin{bmatrix} \boldsymbol{s}_1^T \\ \cdots \\ \boldsymbol{s}_r^T \end{bmatrix} + \boldsymbol{N} \end{aligned} \tag{7}$$

where each $m \times 1$ column vector $\boldsymbol{a}(\rho_i, \boldsymbol{u}_i) \equiv \boldsymbol{G}(\rho_i)\boldsymbol{u}_i$ represents the ith independent topography corresponding to the ith time series $\boldsymbol{s}_i$. The set ρ comprises the $\boldsymbol{r}$ sets of source locations $\{\rho_i\}$ and the set $\boldsymbol{u}$ the corresponding topography orientations $\{\boldsymbol{u}_i\}$. By definition, the matrix of time series $\boldsymbol{S}$ is rank r, and the matrix of topographies $\boldsymbol{A}(\rho, \boldsymbol{u})$ is assumed to be unambiguous and therefore also of rank r. The matrix $\boldsymbol{N}$ represents additive noise, which we will assume to be zero mean and spatially and temporally white with variance σ_e^2. The case of colored noise is readily handled by "prewhitening" of the data and model ([12], [13]).

C. Task and Control Spatiotemporal Measurements

We assume a paired study comprises a *Task* and a *Control* component. The Task measurements are represented by the matrix $\boldsymbol{F}_T$, and we assume that the Task contains p_T independent sources. Similarly, we assume the Control measurement matrix $\boldsymbol{F}_C$ contains p_C independent sources. We also assume that sources active in the Control data are also active in the Task data such that $p_T \geq p_C$. The number of sources present only in the Task data, which we will refer to in the following as the *Target* sources, is $p_D = p_T - p_C$. In practice, it is likely that the Control data may also contain sources which are not present in the Task data. In order to maintain reasonable notation, we have not generalized the development for this case, but it can be handled using a simple modification of the method as discussed in Section III.

Under the assumption that the signal is not correlated with the noise, the autocorrelation matrix for the Control data is

$$\boldsymbol{R}_C = \boldsymbol{E}\{\boldsymbol{F}_C\boldsymbol{F}_C^T\} = \boldsymbol{A}_C(\boldsymbol{S}_C^T\boldsymbol{S}_C)\boldsymbol{A}_C^T + \sigma_{Ce}^2 \cdot \boldsymbol{I} \tag{8}$$

and similarly for the Task data

$$\boldsymbol{R}_T = \boldsymbol{E}\{\boldsymbol{F}_T\boldsymbol{F}_T^T\} = \boldsymbol{A}_T(\boldsymbol{S}_T^T\boldsymbol{S}_T)\boldsymbol{A}_T^T + \sigma_{Te}^2 \cdot \boldsymbol{I}. \tag{9}$$

The corresponding eigendecomposition of these matrices can be represented as follows:

$$\boldsymbol{R}_C = [\Phi_{Cs}|\Phi_{Ce}] \begin{bmatrix} \Lambda_{Cs} & \boldsymbol{0} \\ \boldsymbol{0} & \Lambda_{Ce} \end{bmatrix} [\Phi_{Cs}^T|\Phi_{Ce}^T] \tag{10}$$

$$\boldsymbol{R}_T = [\Phi_{Ts}|\Phi_{Te}] \begin{bmatrix} \Lambda_{Ts} & \boldsymbol{0} \\ \boldsymbol{0} & \Lambda_{Te} \end{bmatrix} [\Phi_{Ts}^T|\Phi_{Te}^T] \tag{11}$$

where in either data set the diagonal matrix $\Lambda_s = \Lambda + \sigma_e^2 \cdot \boldsymbol{I}$ represents p_C the (or p_T) largest "signal plus noise" eigenvalues. Their corresponding orthonormal eigenvectors form the matrix Φ_s. The diagonal matrix $\Lambda_e = (\sigma_e^2 \cdot \boldsymbol{I})$ represents the smallest "noise" eigenvalues and their corresponding eigenvectors form the matrix Φ_e. Using the standard terminology, we will refer to the space spanned by Φ_s as the *signal subspace* and that spanned by Φ_e as the *noise-only subspace*.

In practice, we are limited to a finite set n of temporal samples in $\boldsymbol{F}$ and the signal $\hat{\Phi}_s$ and noise $\hat{\Phi}_e$ subspace basis vectors must be estimated by eigendecomposition of the outer product

$$\hat{\boldsymbol{R}} = \boldsymbol{F}\boldsymbol{F}^T = \left[\hat{\Phi}_s \middle| \hat{\Phi}_e\right] \begin{bmatrix} \hat{\Lambda}_s & 0 \\ 0 & \hat{\Lambda}_e \end{bmatrix} \left[\hat{\Phi}_s^T \middle| \hat{\Phi}_e^T\right]. \tag{12}$$

Alternatively, the spatiotemporal data matrix may be decomposed directly via the SVD as $\boldsymbol{F} = [\hat{\Phi}_s|\hat{\Phi}_e]\hat{\Sigma}\hat{\Psi}^T$ to obtain the same singular vectors $[\hat{\Phi}_s|\hat{\Phi}_e]$, where the eigenvalues are the square of the singular values $\hat{\Sigma}^2 = \hat{\Lambda}$.

III. Methods

A. RAP-MUSIC

Before describing the algorithm for paired data sets, we first summarize the RAP-MUSIC algorithm in [14], an extension of the original MUSIC algorithm [4], [5], [11]. The first source is found as the source location that maximizes the metric

$$\hat{\rho}_1 = \text{argmax}(subcorr(\boldsymbol{G}(\rho), \hat{\Phi}_s)_1) \tag{13}$$

over the allowed source space. The matrix $\boldsymbol{G}(\rho)$ is the gain matrix for the first source, $\hat{\Phi}_s$ is the matrix spanning the estimated signal subspace of the data, and we assume that all appropriate forward modeling assumptions of head and sensors have been incorporated into the gain matrix. The function $subcorr(\bullet)_1$ is the cosine of the first *principal angle* between the subspaces

spanned by the columns of $\boldsymbol{G}(\rho)$ and $\hat{\Phi}_s$. Principal angles are defined in [15]; applications in the context of dipole localization are described in [11] and [14]. For descriptive purposes, we will refer to the cosines of the principle angles as *subspace correlations*.

If we define $\boldsymbol{U_G}$ to be the orthogonal matrix spanning the same space as $\boldsymbol{G}(\rho)$, then the square of the subspace correlations are found as the eigenvalues of the matrix (cf. [5], [11], and [14])

$$\boldsymbol{U}_{\boldsymbol{G}}^T \hat{\Phi}_s \hat{\Phi}_s^T \boldsymbol{U_G}. \tag{14}$$

By maximizing the subspace correlation in (13), we identify the source location ρ and corresponding gain matrix that has the smallest principal angle with respect to the estimated signal subspace. To complete the first independent topography model, we need the corresponding source orientation vector, which is a simple linear transformation of the eigenvector of (14) corresponding to the maximum eigenvalue; see [11] for details. The resulting estimates yield the first estimated independent topography, $\boldsymbol{a}(\hat{\rho}_1, \hat{\boldsymbol{u}}_1) = \boldsymbol{G}(\hat{\rho}_1)\hat{\boldsymbol{u}}_1$.

For the kth RAP-MUSIC recursion, $k = 1, 2, \ldots, r$, the nonlinear source location parameters are found as

$$\hat{\rho}_k = \text{argmax}\left(subcorr\left(\Pi^{\perp}_{\hat{A}_{k-1}} \boldsymbol{G}(\rho), \Pi^{\perp}_{\hat{A}_{k-1}} \hat{\Phi}_S \right)_1 \right) \tag{15}$$

where

$$\hat{\boldsymbol{A}}_{k-1} = [\boldsymbol{a}(\hat{\rho}_1, \hat{\boldsymbol{u}}_1) \quad \cdots \quad \boldsymbol{a}(\hat{\rho}_{k-1}, \hat{\boldsymbol{u}}_{k-1})] \tag{16}$$

represents the independent topography matrix found through the previous recursion. The orthogonal projection operator $\Pi^{\perp}_{\hat{A}_{k-1}}$ is computed as

$$\Pi^{\perp}_{\hat{A}_{k-1}} = \boldsymbol{I} - \hat{\boldsymbol{A}}_{k-1} \hat{\boldsymbol{A}}^{\dagger}_{k-1} \tag{17}$$

where $\hat{\boldsymbol{A}}^{\dagger}_{k-1} = (\hat{\boldsymbol{A}}^T_{k-1} \hat{\boldsymbol{A}}_{k-1})^{-1} \hat{\boldsymbol{A}}^T_{k-1}$ is the pseudo-inverse of $\hat{\boldsymbol{A}}_{k-1}$, and we initialize the topography matrix as $\hat{\boldsymbol{A}}_0$ equal to the "null matrix" and therefore $\Pi^{\perp}_{\hat{A}_0} = \boldsymbol{I}$.

At each iteration, the source location set ρ in (15) may represent one or more dipolar sources. Here, we will restrict the search to one-dipolar models only, halting the recursion when the one-dipolar maximum subspace correlation drops too low. Extensions to multiple synchronous sources are discussed in [11], [14] in which the complexity of the model is increased as the simpler models fall below a correlation threshold.

With all sources in the data identified and their independent topographies represented in the final topography matrix, $\hat{\boldsymbol{A}}_r$ can be used to estimate the corresponding time series

$$\hat{\boldsymbol{S}} = (\hat{\boldsymbol{A}}_r^T \hat{\boldsymbol{A}}_r)^{-1} \hat{\boldsymbol{A}}_r^T \boldsymbol{F} = \hat{\boldsymbol{A}}^{\dagger} \boldsymbol{F}. \tag{18}$$

B. Paired RAP-MUSIC Algorithm

Each iteration of the RAP-MUSIC algorithm begins by projecting both the signal subspace and the model into a reduced dimensional subspace "away" from the existing solution set. This orthogonal projection operation of the existing solution set is easily extended to include the subspace associated with the Control data. We will continue to assume that the distinct Target activity is represented by one-dipolar independent topographies, but we will allow the sources in the Control data to be more generally specified as p_C independent topographies, where each topography may be arbitrarily specified, e.g., a synchronous nondipolar distributed source. We continue to assume that this same set of independent topographies is also present in the Task data, so that the p_T independent topographies in the Task data contain p_C arbitrary independent topographies in common with the Control data and p_D Target one-dipolar topographies, $p_T = p_C + p_D$.

We estimate the two signal subspaces as in (10) and (11), then initialize the RAP-MUSIC algorithm for the Task data with $\hat{\boldsymbol{A}}_0 = \hat{\Phi}_{Cs}$. In other words, we use the estimated signal subspace from the Control data as a "prior data subspace" in the initial recursion of the Task data. For the kth Paired RAP-MUSIC recursion, the algorithm proceeds as before, with (16) modified to be

$$\hat{\boldsymbol{A}}_{k-1} = \begin{cases} \hat{\Phi}_{Cs} & k = 1 \\ \left[\hat{\Phi}_{Cs} \middle| [\boldsymbol{a}(\hat{\rho}_1, \hat{\boldsymbol{u}}_1) \quad \cdots \quad \boldsymbol{a}(\hat{\rho}_{k-1}, \hat{\boldsymbol{u}}_{k-1})] \right] & k = 2, 3, \cdots. \end{cases} \tag{19}$$

The recursion halts after the last source unique to the Task data is identified, i.e., after p_D recursions under our assumption of p_D one-dipolar sources. A flow chart summarizing the Paired RAP-MUSIC algorithm methodology is shown in Fig. 1.

With all distinct Target sources identified, estimates of the corresponding time series associated with just Target source activity can be determined as

$$\hat{\boldsymbol{S}} = (\Pi^{\perp}_{\hat{A}_0} \hat{\boldsymbol{A}}_D)^{\dagger} \Pi^{\perp}_{\hat{A}_0} \boldsymbol{F}_T \tag{20}$$

where $\hat{\boldsymbol{A}} = [\boldsymbol{a}(\hat{\rho}_1, \hat{\boldsymbol{u}}_1) \cdots (\hat{\rho}_k, \hat{\boldsymbol{u}}_k)]$ is the submatrix in (19) representing the Target topographies found during the paired RAP MUSIC search.

C. Extensions

In the description above and in the simulations and experiments that follow, we have considered the case where the Control sources are also present in the Task data. We have additionally assumed that the correct rank of the Control and Task are selected when forming the signal subspace estimates. We now describe extensions of the Paired RAP-MUSIC algorithm to the case of distinct activity in both the Control and Task data, as well as overspecified ranks of both signal subspaces.

The rank of the signal subspace is typically selected by visual inspection of the singular value spectrum (e.g., [5], [11]). If there is not a clear drop in the singular values to clearly indicate the rank, then it is safer to overestimate the assumed rank.

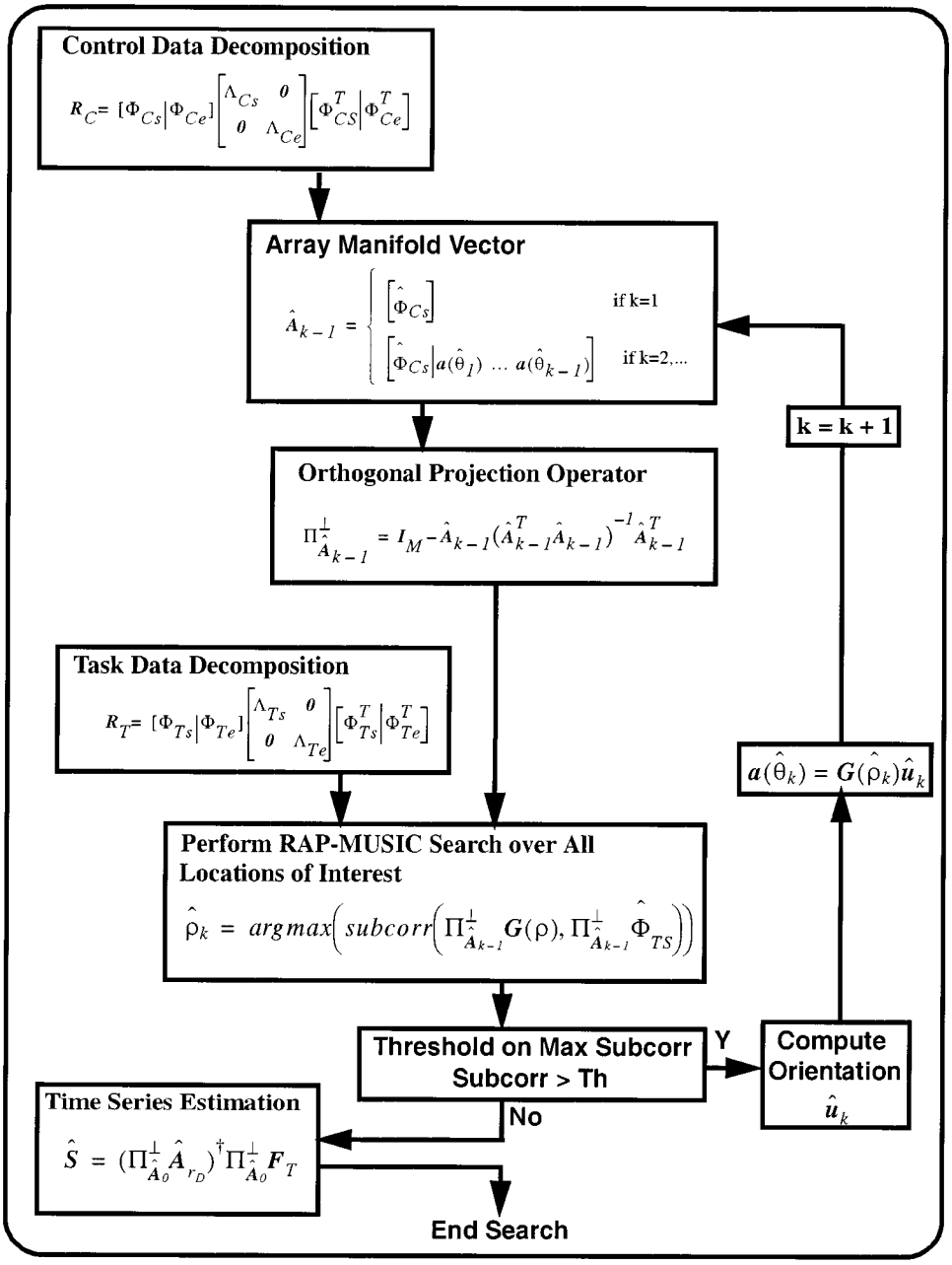

Fig. 1. Paired RAP MUSIC algorithm flow chart.

Selecting too large a rank will result in additional "noise" eigenvectors being included in the signal subspace estimate; however, the probability is quite small that these additional noise eigenvectors will actually correlate with the source models (cf. [16]). Conversely, selecting too small a rank can be detrimental, in some cases resulting in an inability to localize any sources. In this extension, we will therefore assume that the ranks p_C and p_T for the Control and Task data may be overspecified. The number of distinct Target one-dipolar independent topographies remains designated as p_D, but in this extension this number may no longer be the simple difference between p_C and p_T.

The Paired RAP-MUSIC algorithm described in the previous section may still be used even in the case where the Control subspace contains these additional eigenvectors. When the method is applied, however, the projection of the Task signal subspace away from the additional eigenvectors may unnecessarily suppress signal energy in the distinct Target sources. Consequently, localization accuracy of the Target sources may needlessly suffer. We can instead find the component of the Control subspace which is also in the Task subspace, and project away from only this component in (19). We identify this common subspace from the subspace correlations between the two spaces as

$$subcorr(\hat{\Phi}_{Cs}, \hat{\Phi}_{Ts}). \tag{21}$$

In the noiseless case, if the Control sources are all present in the Task data, then the rank p_C of the Control data is less than

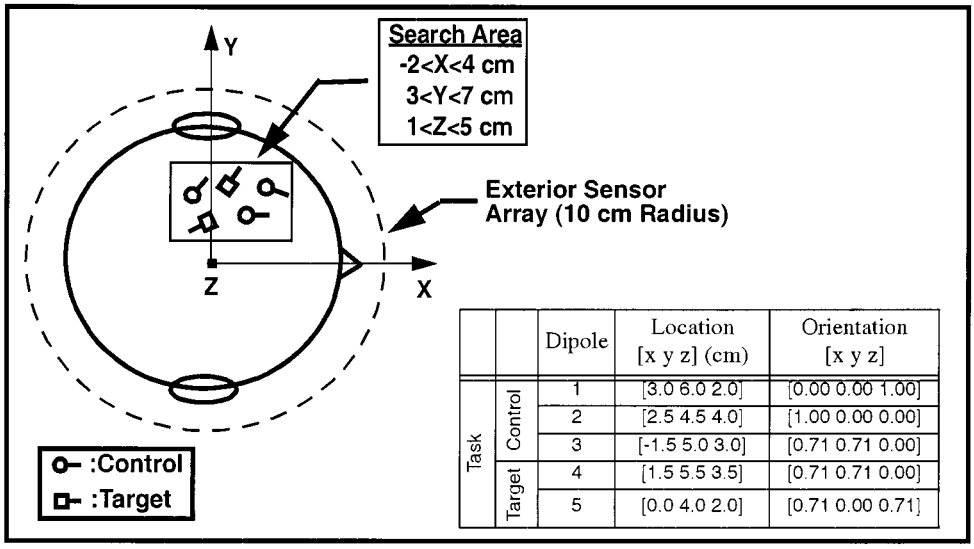

		Dipole	Location [x y z] (cm)	Orientation [x y z]
Task	Control	1	[3.0 6.0 2.0]	[0.00 0.00 1.00]
		2	[2.5 4.5 4.0]	[1.00 0.00 0.00]
		3	[-1.5 5.0 3.0]	[0.71 0.71 0.00]
	Target	4	[1.5 5.5 3.5]	[0.71 0.71 0.00]
		5	[0.0 4.0 2.0]	[0.71 0.00 0.71]

Fig. 2. Source locations, orientations, and search limit boundaries used in computer simulation.

the rank p_T of the Task data, and the analysis will reveal p_C subspace correlations equal to unity. In the presence of moderate noise, these p_C correlations will be near unity. In the case where the Control subspace contains additional sources not found in the Task data, then only a subset of the subspace correlations will be near unity. More generally, we will find k correlations near unity, where $k \leq \min(p_C, p_T)$. These k correlations correspond to a k-dimensional subspace common to the two signal subspaces in (21). As described in [11], [15], the corresponding k *principal vectors* from each signal subspace are readily identified as part of the subspace correlation calculation. We can form the common subspace $\hat{\Phi}_{TCs}$ from the corresponding principal vectors in the Control data and use this subspace in place of $\hat{\Phi}_{Cs}$ in (19).

With the common subspace identified, Paired RAP-MUSIC proceeds as above to identify the distinct Target activity in the Test data, halting after p_D recursions of a one-dipolar topography. Note that this procedure does not estimate the activity distinct to the Control data. To model the distinct Control activity, we simply reverse the role of Task and Control in the above discussion.

IV. Simulation Studies

A. Dipolar Source Study

In order to assess the viability of the proposed method, we performed a multiepoch Monte Carlo simulation. This simulation employed a 64-sensor hemispherical array with data collected over 100 epochs. Each epoch comprised 500 time samples and the amplitude and latency were varied between epochs. One hundred independent Monte Carlo trials were performed.

MEG Array Geometry: We simulated an array of 64 radially oriented magnetometers along the outer circumference of a 10-cm hemisphere. The sensors were nominally uniformly spaced with approximately 3.8 cm between sensors.

Multiepoch Current Dipole Time Series Generation: Five dipolar sources were generated with linearly independent time series. Our goal was to generate realistically shaped overlapping time series possessing moderate cross correlations (0.3–0.6). The dipole time series were generated using exponentially decaying sinusoids of varying frequencies to simulate the shapes of the time series shown for example in [8]. A total of 500 samples were generated for each time series using a sample rate of 1 ms. Location and orientation were assumed to be fixed for each dipole. A peak dipole moment of 10 nA-m was used for each dipole. The location and orientation of each dipole is summarized in Fig. 2. A plot of the time series for each dipole is shown in Fig. 3.

A total of 100 epochs were generated for each Monte Carlo trial. Each epoch was allowed to vary in both amplitude and latency. Latency variations were Gaussian with a standard deviation of 10 ms. Amplitude variations were generated using a uniformly distributed scaling factor between 0.5–1.5, yielding peak dipole moments between 5–15 nA-m. A depiction of the first ten epochs in the presence of amplitude and latency variations is shown in Fig. 3.

Sensor Measurement Generation: Radially oriented magnetic field measurements were generated and white Gaussian noise added to each measurement sample. Two different noise levels were investigated in this study (see Table I). The single-epoch SNR is defined as the square of the Frobenius Norm (F-norm) of the noiseless signal matrix divided by the square of the F-norm of the noise-only data matrix. The spatiotemporal matrix used for source localization was obtained by averaging over all epochs, as shown in Fig. 4. The effective SNR following averaging is increased in proportion to the number of trials.

Baseline RAP-MUSIC Localization: The RAP-MUSIC algorithm described in Section III was used to localize each of the five sources on a 0.05-cm grid in the range: $-2.0 \leq x \leq 4.0$ cm; $3.0 \leq y \leq 7.0$ cm; and $1.0 \leq z \leq 5.0$ cm. A dipole localization was declared for a maximum subspace correlation greater than 0.95. In order to maintain consistency throughout this study, the rank of the data matrix signal subspace was al-

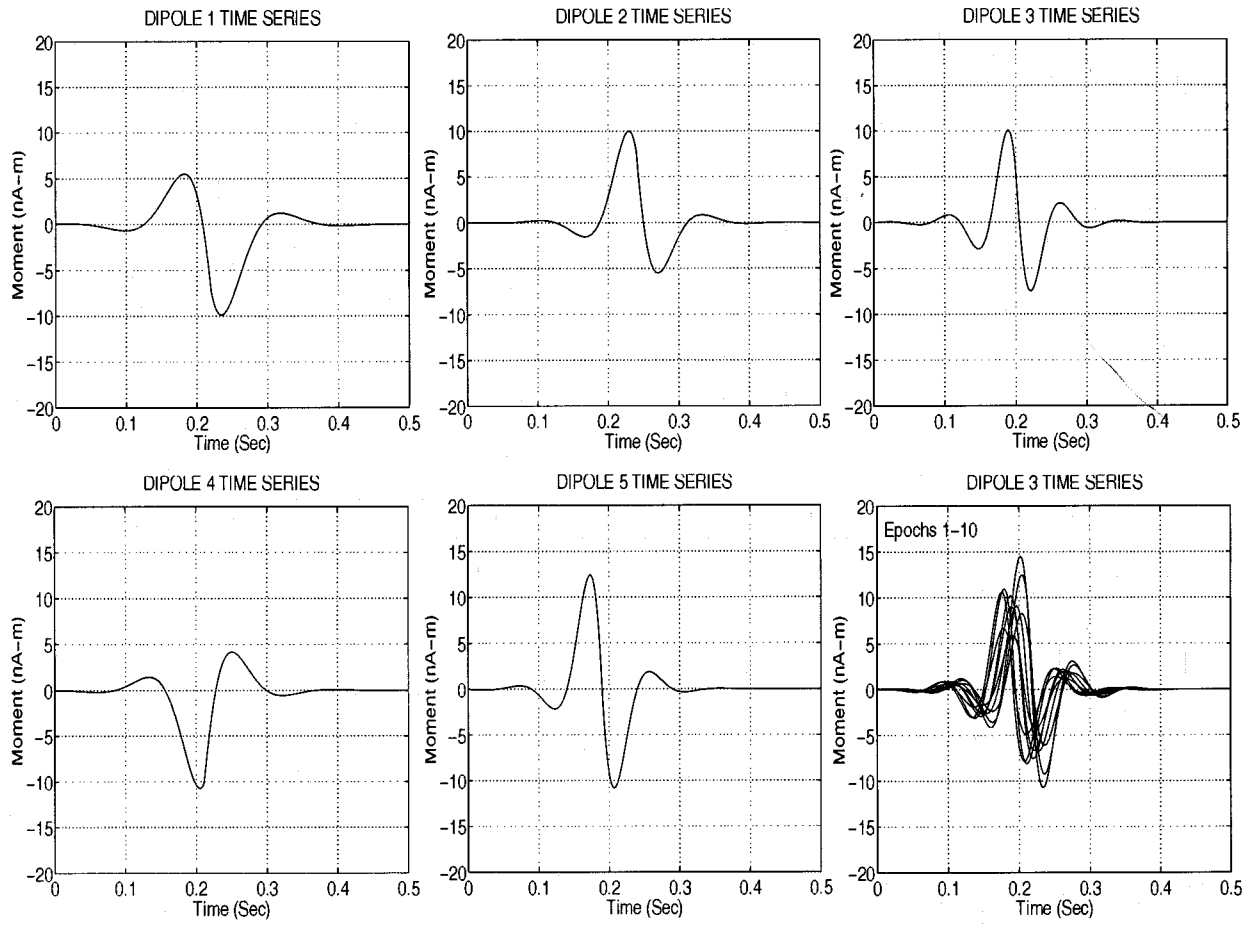

Fig. 3. Dipole source time series used in computer simulation. Control set consists of dipoles 1–3 shown on top row. Target dipole set consists of dipoles 4–5 on bottom row. Example of epoch-to-epoch amplitude/latency variations is shown for first ten epochs of dipole 3 in lower right plot.

ways correctly specified; see the Extensions section above for discussions on overspecifying the rank.

The RAP-MUSIC localization procedure was repeated for each of 100 Monte Carlo trials. The mean and standard deviation of each of the following metrics was computed.

1) Localization Accuracy: Vector distance $\varepsilon = \|\hat{\boldsymbol{r}}_q - \boldsymbol{r}_q\|$ between the true dipole location $\boldsymbol{r_q}$ and the localization estimate $\hat{\boldsymbol{r}}_{\boldsymbol{q}}$.
2) Subspace Correlation: Cosine of the smallest principle angle between the signal subspace $\hat{\Phi}_s$ spanned by the data and the subspace spanned by the forward model $\boldsymbol{G}(\hat{\rho})$ at the location $\hat{\rho}$.

Localization results for this case are shown in Table I. Standard deviations in the localization errors ranged from fractions of a millimeter in the high SNR case up to 3.7 mm for the weakest dipole in the lower SNR case. In all cases, a very strong subspace correlation (greater than 0.99) was observed.

Paired RAP-MUSIC Localization: Task data were identical to that used in the above baseline study. The Control data were generated using dipoles 1 to 3 only. The Control data were generated independently from the Task using different realizations of the noise, dipole latency, and amplitude variations. Localization results after projecting the Task signal subspace away from the Control subspace are summarized in the second result column in Table I. In each case, sources in the Control data were effectively blocked while Target sources were successfully localized. Localization accuracy of Target dipoles 4 and 5 using the paired data was found to be nearly identical to that obtained via direct localization on the 5-dipole Task data-set. In nearly all cases, the difference in localization error between the two results was within 1 mm. Direct extraction of Target Source time-series activity utilizing equation (20) is shown in Fig. 5, where the extracted target dipole time series is plotted alongside the true dipole time-series. This figure demonstrates the ability of the paired RAP MUSIC method to successfully extract the Target time series even when they are partially correlated with the sources in the Control data.

For comparison, we also performed a localization study using the Covariance Difference method described in [3]. For this study the sources in Control and Test were identical to those used in the Paired RAP MUSIC study except that the dipole time series was fixed for all epochs (i.e., no amplitude or latency variations). In addition, a RAP-MUSIC search was employed rather than a classical MUSIC search. Localization results for this experiment are presented in the final result column in Table I. While Control source activity was successfully blocked, only one of the two Target sources was successfully localized. The error associated with this localization was in excess of 1 cm. In

TABLE I
RAP-MUSIC DIPOLE SEARCH RESULTS USING FIVE ONE-DIPOLAR SOURCES IN THE TASK DATA AND THREE ONE-DIPOLAR SOURCES IN THE CONTROL DATA. RESULTS SHOWN FOR DIRECT RAP-MUSIC LOCALIZATION ON TASK DATA, PAIRED RAP-MUSIC LOCALIZATION USING TASK AND CONTROL DATA, AND PAIRED DATA LOCALIZATION USING COVARIANCE DIFFERENCE METHOD [3]. STATISTICS COMPUTED OVER 100 MONTE CARLO TRIALS

		5 Dipole Task data w/ no Control data (RAP-MUSIC)		5 Dipole Task data w/ 3 Dipole Control data (Paired RAP-MUSIC)		5 Dipole Task data w/ 3 Dipole Control data (Covariance Diff Method)	
HIGH SNR CASE							
Dipole	SNR (1-Epoch)	Loc Error (cm) Mean/s.d.	Subspace Correlation Mean/s.d.	Loc Error (cm) Mean/s.d.	Subspace Correlation Mean/s.d	Loc Error (cm) Mean/s.d	Subspace Correlation Mean/s.d
1	0.302	0.0027/ 0.01201	0.9999/ 0.00002	No Detection (Blocked)	No Detection (Blocked)	No Detection (Blocked)	No Detection (Blocked)
2	0.154	0.0464/ 0.04141	0.9994/ 0.00031	No Detection (Blocked)	No Detection (Blocked)	No Detection (Blocked)	No Detection (Blocked)
3	0.089	0.0316/ 0.034437	0.9993/ 0.00026	No Detection (Blocked)	No Detection (Blocked)	No Detection (Blocked)	No Detection (Blocked)
4	0.010	0.0547/ 0.03903	0.9981/ 0.00032	0.0604/ 0.033335	0.9976/ 0.000407	1.1318/ 0.024863	0.9893/ 0.000405
5	0.060	0.0682/ 0.038322	0.9985/ 0.00070	0.0777/ 0.045045	0.9981/ 0.000407	No Detection	No Detection
LOW SNR CASE							
Dipole	SNR (1-Epoch)	Loc Error (cm) Mean/s.d.	Subspace Correlation Mean/s.d.	Loc Error (cm) Mean/s.d.	Subspace Correlation Mean/s.d	Loc Error (cm) Mean/s.d	Subspace Correlation Mean/s.d
1	0.048	0.0887/ 0.041620	0.9992/ 0.000169	No Detection (Blocked)	No Detection (Blocked)	No Detection (Blocked)	No Detection (Blocked)
2	0.025	0.1829/ 0.085843	0.9926/ 0.003657	No Detection (Blocked)	No Detection (Blocked)	No Detection (Blocked)	No Detection (Blocked)
3	0.014	0.1329/ 0.079747	0.9918/ 0.003875	No Detection (Blocked)	No Detection (Blocked)	No Detection (Blocked)	No Detection (Blocked)
4	0.016	0.1743/ 0.077907	0.9854/ 0.003313	0.1861/ 0.091795	0.9832/ 0.003158	1.1242/ 0.031321	0.9881/ 0.001093
5	0.0009	0.3710/ 0.171198	0.9946/ 0.004996	0.2299/ 0.111124	0.9858/ 0.002532	No Detection	No Detection

comparison, localization errors using the Paired RAP-MUSIC method were between 0.1–2.3 mm (Table I).

B. Distributed Source Study

In order to determine the algorithm performance in the presence of more complex distributed sources, a $1 \times 1 \times 1.5$ cm rectangle "distributed current field" was created by generating 27 synchronously activated sources all within the vicinity of dipole 2. The moment of each of these sources was scaled by 27 such that the total source moment remained unchanged.

The results are shown in Table II. Baseline RAP-MUSIC localization was performed on the five source Task data-set. The Paired RAP MUSIC method was then applied to the five source Task data with three source Control data. The single epoch F-Norm SNR of the Task data was on the order of 0.1 (giving a 100-epoch post averaged SNR of approximately ten). A one-dipolar forward model was utilized in the RAP-MUSIC search.

As shown in Table II, the baseline study shows a dipole in the vicinity of the simulated 27-dipole "current field," albeit with a somewhat large localization error of 4.5 mm (the error was computed with respect to the centroid of the distributed source). In the paired experiment, the distributed source was successfully "blocked" with no adverse affect on the localization solution of the Target sources. As was the case with the one-dipolar sources, target source localization accuracy using either direct localization or the Paired RAP-MUSIC method were observed to be nearly equivalent. Paired experiments were also conducted using Control data-sets containing distributed sources containing two or three synchronously activated dipoles. In each case, these distributed source topographies were successfully blocked with no observed degradation in the localization error of Target source activity.

V. PHANTOM EXPERIMENTS

A. Overview

This method was also evaluated using MEG data collected in a controlled phantom experiment. In these experiments, a phantom containing 32 programmable dipoles was used to simultaneously collect EEG and MEG data. MEG data was collected using a Neuromag-122 (Neuromag Ltd., Helsinki, Finland) whole head system at the Neuroimaging Center of the New Mexico Regional Federal Medical Center in Albuquerque, New Mexico. This machine contains 61 dual-channel planar-gradiometer sensors giving a total of 122 spatial measurements. An X-ray computed tomography (CT)-generated side view of the phantom is shown in Fig. 6.

Evaluation of data collected directly from a physical system has the advantage that effects associated with forward model inaccuracies, the nonideal nature of the sensors, and correlated background noise are present in the data. These effects are not well modeled (and often ignored) in simulation studies. The use of phantom data has the secondary advantage that dipole location, orientation, and time-series "ground truth" can be established. In this study, true dipole locations and orientations

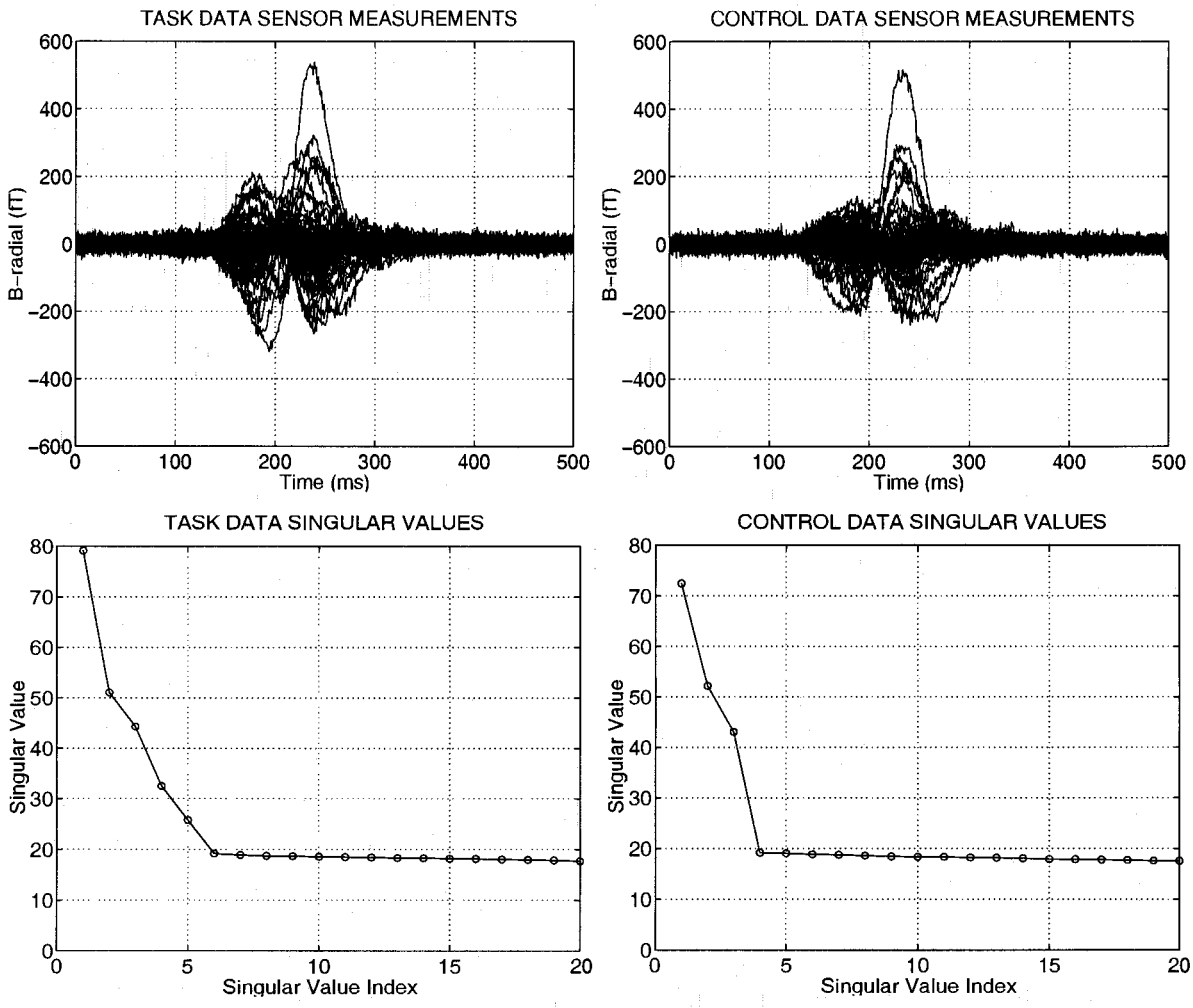

Fig. 4. Computer simulation Task (upper left) and Control (upper right) waveform sets. Each plot shows radial magnetic field measurement for each of the 64 sensors averaged over 100 epochs. The 20 largest singular values corresponding to the Task data (lower left) and the Control data (lower-right) are shown for a low SNR case.

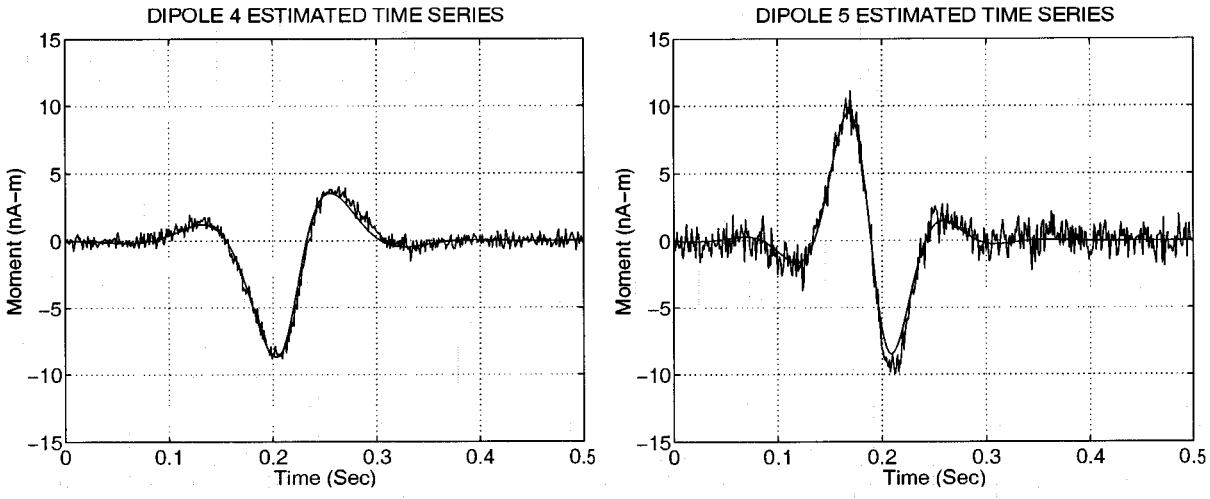

Fig. 5. Plot of recovered time series for Target sources 4 and 5 using computer simulation data described in Section IV. Task data consisted of five 1-dipolar sources while Control data consisted of three 1-dipolar sources. Time series estimated using equation (20).

were extracted from X-ray CT scans of the phantom and the dipole time series were those used in the source file for the programmable dipole driver. A comprehensive description of the phantom physical model, experimental observations, and indi-

TABLE II
PAIRED RAP-MUSIC DIPOLE SEARCH RESULTS USING TASK DATA (CONTAINING ONE DISTRIBUTED SOURCE & FOUR ONE-DIPOLAR SOURCES) WITH CONTROL DATA (CONTAINING ONE DISTRIBUTED SOURCE & TWO ONE-DIPOLAR SOURCES). STATISTICS COMPUTED OVER 100 MONTE CARLO TRIALS

		5 Source Task data w/ no Control data (RAP-MUSIC)		5 Source Task data w/ 3 Source Control data (Paired RAP-MUSIC)	
Source	SNR (1-Epoch)	Loc Error (cm) Mean/s.d.	Subcorr Mean/s.d.	Loc Error (cm) Mean/s.d.	Subcorr Mean/s.d.
1	0.033	0.1444/ 0.046136	0.9988/ 0.000212	No Detections (Blocked)	No Detections (Blocked)
2 (Dist Source)	0.017	0.4468/ 0.096436	0.9839/ 0.002724	No Detections (Blocked)	No Detections (Blocked)
3	0.001	0.2366/ 0.19779	0.9718/ 0.008129	No Detections (Blocked)	No Detections (Blocked)
4	0.011	0.2470/ 0.107836	0.9654/ 0.007778	0.2012/ 0.094013	0.9684/ 0.005620
5	0.008	0.6034/ 0.117227	0.9959/ 0.006228	0.3203/ 0.169079	0.9703/ 0.005874

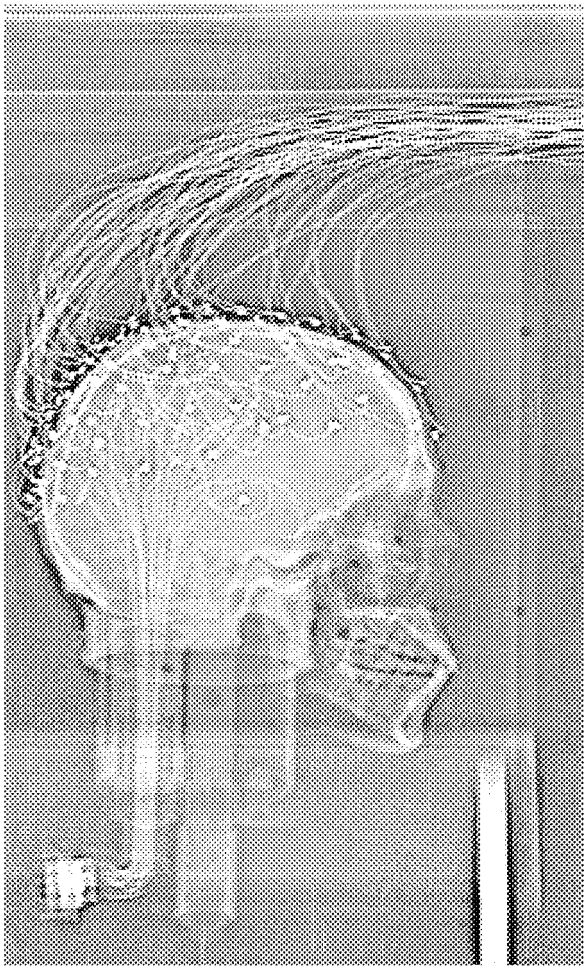

Fig. 6. X-ray CT view of skull phantom and EEG electrodes. The tips of the 32 coaxial cables inserted through the base form the individual dipoles. The opposite end of the cables were connected to the source driver via a connector (shown in the lower left).

vidual dipole localization results are described by Leahy *et al.* [17].

In the phantom study, each of the 32 dipoles was driven using a 10-Hz sinusoid. Dipoles were fired in succession (with no overlap) so that the activation time for each dipole was 1.0 s. The estimated peak amplitude of each dipole was between 200–300 nA-m. MEG measurements were sampled at a rate of 500 samples/s. Observed SNRs for the subset of dipoles used in this study (expressed as the square of the F-Norm of the spatiotemporal data matrix divided by the square of the F-Norm of "noise-only" data collected under prestimulus conditions) were in the range of 5.9–10.9. These SNRs represent single-epoch values computed from data sets which included all post-filtering operations. All phantom localization experiments in this paper were performed using one epoch of data. It should be noted that this data is somewhat noisier than data collected in a typical MEG experiment where spatiotemporal data-sets are averaged over multiple epochs to smooth out uncorrelated background noise. Raw data collected on the phantom showed significant signs of 60 Hz background noise interference. To minimize the effects of this noise, the raw data sets were filtered using a four-pole elliptic low-pass filter with a cutoff frequency of 20 Hz. In [17] the dipole localization errors due to registration of the MEG data to the X-ray CT images of the phantom and to extraction of the dipole locations from the CT images were estimated to be 2–3 mm. All localization experiments presented in this paper utilized a RAP-MUSIC search incorporating a single locally fitted sphere forward model [10].

B. Phantom Localization Experiments

Spatiotemporal data collected in the phantom experiment described above were used to construct multiple dipole data-sets possessing correlated time sequences. Given two dipoles with sinusoidal time-series of the same frequency, the desired cross correlation was obtained by adding an appropriate phase shift. This technique was limited to two sinusoidal time-series since a third phase-shifted sinusoid can be represented as a linear combination of the other two. Additional data-sets were created by resampling the original 10-Hz time series to 5.71 Hz. Using this technique, a set of four dipoles were constructed. The time-series cross correlation was 0.41 between dipoles 1 and 3 and 0.54 between dipoles 2 and 4.

Multiple dipole data sets were constructed by adding together the time-series associated with each of the dipoles of interest. In order to avoid any potential transient effects that may have occurred at the time of dipole switching during the original phantom study, only the central 800 ms (400 samples) of the

TABLE III
PHANTOM STUDY: RAP-MUSIC DIPOLE SEARCH RESULTS USING FOUR ONE-DIPOLAR TASK DATA AND TWO ONE-DIPOLAR CONTROL DATA. RESULTS SHOWN FOR DIRECT RAP-MUSIC LOCALIZATION ON TASK DATA AND PAIRED RAP-MUSIC LOCALIZATION USING TASK AND CONTROL DATA

		4 Dipole Task data w/ no Control data (RAP-MUSIC)		4 -Dipole Task data w/ 2-Dipole Control data (Paired RAP-MUSIC)	
Dipole	True Dipole Location [x y z] cm	Localization Error (cm)	Subcorr	Localization Error (cm)	Subcorr
1	[-3.90 2.25 2.64]	0.77	0.9225	No Detection (Blocked)	No Detection (Blocked)
2	[-3.95 0.93 3.83]	0.41	0.9930	No Detection (Blocked)	No Detection (Blocked)
3	[-2.68 1.18 4.60]	0.58	0.9614	0.32	0.9491
4	[-3.03 -0.45 4.04]	0.10	0.9887	0.37	0.9769

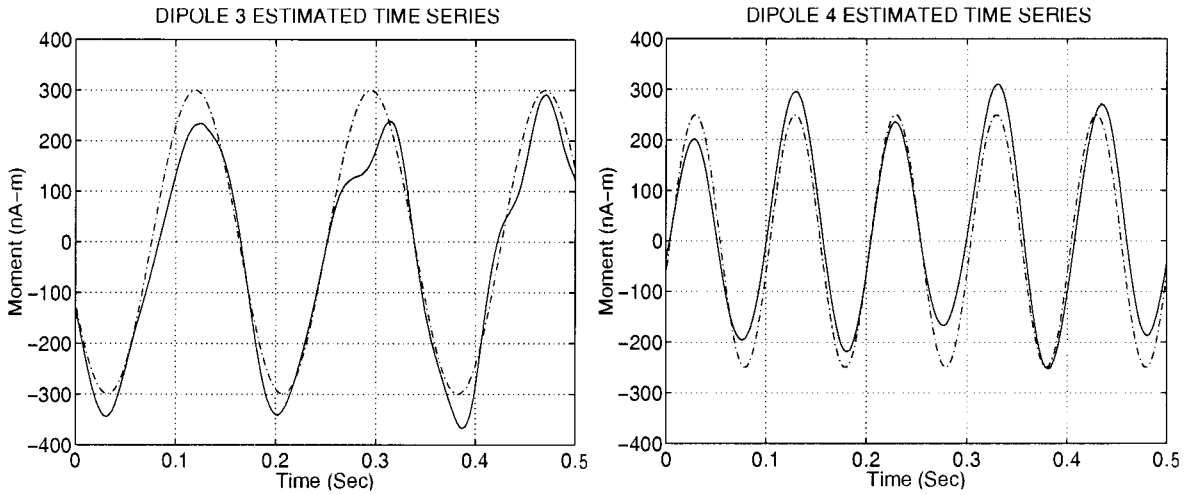

Fig. 7. Plot of recovered time series for target sources 2 and 3 using low SNR single-epoch phantom data for the case summarized in Table III. Task data consisted of four 1-dipolar sources while Control data consisted of two 1-dipolar sources. Time series estimation performed using equation (20). A 10-Hz and 5.71-Hz sinusoid (representing the true time series) are shown for reference with a broken line.

TABLE IV
RAP-MUSIC DIPOLE SEARCH RESULTS USING TWO ONE-DIPOLAR AND ONE TWO-DIPOLAR SOURCE IN TASK DATA AND ONE ONE-DIPOLAR AND ONE TWO-DIPOLAR SOURCE IN CONTROL DATA. RESULTS SHOWN FOR DIRECT RAP-MUSIC LOCALIZATION ON TASK DATA AND PAIRED RAP-MUSIC LOCALIZATION USING TASK AND CONTROL DATA

		4-Source Task data w/ no Control data (RAP-MUSIC)		4- Source Task data w/ 2-Source Control data (Paired RAP-MUSIC)	
Source	True Source Location [x y z] cm	Localization Error (cm)	Subcorr	Localization Error (cm)	Subcorr
1 (2-Dipolar)	[-3.90 2.25 2.64] [-3.03 -0.45 4.04]	1.01	0.9410	No Detection (Blocked)	No Detection (Blocked)
2	[-2.68 1.18 4.60]	0.45	0.9917	No Detection (Blocked)	No Detection (Blocked)
3	[-4.17 2.73 2.10]	0.26	0.9882	0.35	0.9653

each 1.0-s data set were utilized. To ensure that Task and Control data sets each contained independent noise samples, a separate dipole time-series realization was utilized in each data set. The results of two localization experiments using correlated Task and Control data are shown in Table III for a case using dipoles 1–4 in the Task data and dipoles 1 and 2 in the Control data. Baseline localization using the Task data was able to locate all four dipoles. The paired RAP MUSIC search using the Control data to block dipoles 1 and 2 resulted in detection of dipoles 3 and 4. When compared to the phantom truth data, the localization error using the Paired-RAP method showed a slight increase (2.7 mm) in the case of dipole 4 and a slight decrease (2.4 mm) in the case of dipole 3. The time series for the two Target sources in the Task data are shown in Fig. 7. Note that the method is able to extract the Target time courses even when they are correlated with the sources in the Control.

A second example used two synchronous dipoles and one independent dipole in the Control, as shown in Table IV. The

Task data contained these sources plus a second dipole. Again, the Paired RAP MUSIC method was able to localize the Target source in the Task data. In this case, a slight increase in error (1 mm) was observed. In both examples, a slight decrease in the subspace correlation using the Paired RAP-MUSIC method was also observed.

VI. Conclusion

We have presented a new method for extracting source activity from paired MEG data where the objective is to identify source activity occurring in the Task data but not in the Control. The method presented is based on the RAP-MUSIC algorithm, a variant of the well-known MUSIC algorithm. A key feature of the RAP-MUSIC algorithm is the orthogonal projection operator which effectively "removes" the subspace associated with previously located source activity. In the Paired RAP-MUSIC method, the orthogonal projection operation is extended to include the signal subspace of the Control data.

Computer simulation and phantom studies show the Paired RAP-MUSIC method is effective at blocking out Control source activity and identifying Target source activity. In addition to simple point-dipolar sources, effective blocking of more complicated sources was demonstrated. Synchronously activated sources present a challenge given that their subspace collapses into a subspace different than that of the individual sources. Direct localization of complex sources (using subspace based methods) is often difficult given that the combinatorics associated with testing multiple-dipole forward models is often prohibitive. While distributed source activity may be difficult to localize, knowledge of its subspace is sufficient to effectively block the source via application of the orthogonal projection operator.

Localization accuracy of Target source activity using the Paired RAP-MUSIC method was found to be nearly equivalent to results obtained by performing direct RAP-MUSIC localization on the entire Task data-set. In some cases, the paired-RAP method produced superior localization results, whereas in other cases direct localization produced better results. This was observed in both the simulation and phantom studies where differences in localization accuracy were within 3 mm.

Computer simulation and phantom study results show this method to be effective in cases where the cross correlation between Task and Control source time-series was significant (values of 0.3–0.6 were tested in this study). In comparison, the method presented in [3] was shown to be ineffective in cases where source activity possessed significantly correlated time-series. The Paired RAP-MUSIC method was also shown to be effective in the case of a multiepoch computer simulation where random signal "jitter" (amplitude and latency variations) occurs between epochs and data-sets. A straightforward expression for estimating the time-series associated with Target source activity (20) was also presented and validated in simulation and phantom studies.

Although the methods presented in this paper focus on the MEG inverse problem, the results are directly applicable to the EEG inverse problem after application of the appropriate forward model.

References

[1] K. J. Worsley, S. Marrett, P. Neelin, A. C. Vandal, K. J. Friston, and A. C. Evans, "A unified statistical approach for determining significant signals in images of cerebral activation," *Human Brain Mapping*, vol. 4, no. 1, pp. 58–73, 1996.

[2] J. C. Mosher, M. E. Spencer, R. M. Leahy, and P. S. Lewis, "Error bounds for EEG and MEG dipole source localization," *Electroenceph. Clin. Neurophys.*, vol. 86, pp. 303–320, 1993.

[3] K. Sekihara, D. Poeppel, A. Marantz, C. Phillips, H. Koizumi, and Y. Miyashita, "MEG covariance difference analysis: A method to extract target source activities by using task and control measurements," *IEEE Trans. Biomed. Eng*, vol. 45, pp. 87–97, Jan. 1998.

[4] R. O. Schmidt, "Multiple emitter location and signal parameter estimation," *IEEE Trans. Antennas Propagat.*, vol. AP-34, pp. 276–280, Mar. 1986.

[5] J. C. Mosher, P. S. Lewis, and R. M. Leahy, "Multiple dipole modeling and localization from spatio-temporal MEG data," *IEEE Trans. Biomed. Eng*, vol. 39, pp. 541–557, Jun. 1992.

[6] A. C. K. Soong and Z. J. Koles, "Principal component localization of the sources of the background EEG," *IEEE Trans. Biomed. Eng*, vol. 42, pp. 59–67, Jan. 1995.

[7] J. Tripp, "Physical concepts and mathematical models," in *Biomagnetism: An Interdisciplinary Approach*, Williamson, Romani, Kaufman, and Modena, Eds. New York: Plenum, 1983, pp. 101–139.

[8] M. Hämäläinen, R. Hari, R. J. IImoniemi, J. Knuutila, and O. V. Lounasmaa, "Magnetoencephalography-theory, instrumentation, and applications of noninvasive studies of the working human brain," *Rev. Mod. Phys.*, vol. 65, pp. 413–497, Mar. 1993.

[9] J. C. Mosher, R. M. Leahy, and P. S. Lewis, "EEG and MEG: Forward solutions for inverse methods," *IEEE Trans. Biomedical Eng*, pp. 245–259, March 1999.

[10] J. Sarvas, "Basic mathematical and electromagnetic concepts of the biomagnetic inverse problems," *Phys. Med. Biol.*, vol. 32, pp. 11–22, 1987.

[11] J. C. Mosher and R. M. Leahy, "Recursively applied MUSIC: A framework for EEG and MEG source localization," *IEEE Trans. Biomed. Eng*, pp. 1342–1355, Nov. 1998.

[12] H. W. Sorenson, *Parmeter Estimation*. New York: Macrel Dekker, 1980.

[13] K. Sekihara, S. Miyauchi, and H. Koizumi, "Covariance incorporated MEG-MUSIC algorithm and its application to detect SI and SII when large background brain activity exists," *Neuroimage*, vol. 3, no. 3, p. S29, June 1996.

[14] J. C. Mosher and R. M. Leahy, "Source localization using recursively applied and projected (RAP) MUSIC," *IEEE Trans. Signal Processing*, pp. 332–340, Feb. 1999.

[15] G. H. Golub and C. F. Van Loan, *Matrix Computations*, 2nd ed. Baltimore, MD: Johns Hopkins Univ. Press, 1984.

[16] J. Vandewalle and B. De Moor, "A variety of applications of singular value decomposition in identification and signal processing," in *SVD and Signal Processing, Algorithms, Applications, and Architectures*, E. F. Deprettee, Ed. Amsterdam, The Netherlands: Elsevier, 1988, pp. 43–91.

[17] R. M. Leahy, J. C. Mosher, M. E. Spencer, M. X. Huang, and J. D. Lewine, "A study of dipole localization accuracy for MEG and EEG using a human skull phantom," *Electroencephalogr. Clin. Neurophysiol.*, vol. 107, pp. 159–173, Aug. 1998.

John J. Ermer (S'83–M'91) was born in Burbank, CA in 1962. He received the B.S. degree in electrical engineering from California State University, Northridge, in 1985, and the M.S. and E.E.E. degrees in electrical engineering from the University of Southern California, Los Angeles, in 1987 and 1991, respectively. He is currently working toward the Ph.D. degree at the same university in the Signal and Image Processing Institute of the Department of Electrical Engineering-Systems.

Since 1985, he has been with the Airborne Radar division of Hughes Aircraft/Raytheon Systems Company, El Segundo, CA, working on Navigation and Track/ECCM algorithm development. His technical interests are in the area of array signal processing, parameter estimation, and source localization.

John C. Mosher (S'80–M'82) eceived the B.S. degree in electrical engineering with highest honors from the Georgia Institute of Technology, Atlanta, in 1983. From 1979–1983 he was also a cooperative education student with Hughes Aircraft Company, Fullerton, CA. He received the M.S. and Ph.D. degrees in electrical engineering from the Signal & Image Processing Institute of the University of Southern California in 1985 and 1993, respectively.

From 1983–1993, he worked at TRW, Los Angeles, CA, researching signal analysis procedures for electromagnetic pulse effects. Upon graduation, he accepted a staff position at the Los Alamos National Laboratory, Los Alamos, NM, where he researches the forward and inverse modeling problems of electrophysiological recordings. A member of the Design Technology Group, his interests also include the general source localization and imaging problems, both in neuroscience work and in other novel applications of sensor technology.

Mingxiong Huang received the Ph.D. degree in biomedical physics in 1995 from Northeastern University, Boston, MA.

He was a Postdoctoral Research Associate from 1995–1997 at Los Alamos National Laboratory. He is currently a Research Assistant Professor in Department of Radiology, University of New Mexico, Albuquerque, NM, and Research Scientist at VA Medical Center, Albuquerque, NM. His major research interests are forward and inverse problems of magnetoencephalography (MEG) and electroencephalography (EEG), and using MEG and EEG to study normal and abnormal brain functions.

Richard M. Leahy (M'85) was born in Surrey, England, in 1960. He received the B.Sc. and Ph.D. degrees in electrical engineering from the University of Newcastle upon Tyne, England in 1981 and 1985, respectively.

In 1985 he joined the University of Southern California (USC), Los Angeles, where he is currently a Professor in the Department of Electrical Engineering—Systems and Director of the Signal and Image Processing Institute. He holds joint appointments with the Departments of Radiology and Biomedical Engineering at USC. His research interests lie in the application of signal and image processing theory to biomedical inverse problems. His current research involves the development of methods for anatomical and functional imaging with applications in neuroimaging and oncology.

Dr. Leahy is an Associate Editor of the IEEE TRANSACTIONS ON MEDICAL IMAGING and was Associate Chair of the IEEE Conference on Medical Imaging in 1992 and 1993.